AIAA Aviation and Aeronautics Forum and Exposition 2016
Jun 13-17, 2016, Washington, DC.

Processing Near-Infrared Imagery of the Orion Heatshield During EFT-1 Hypersonic Reentry

Thomas S. Spisz[1], Jeff C. Taylor[2], David M. Gibson[3], Steve Kennerly[4], and Kwame Osei-Wusu[5]
Johns Hopkins University Applied Physics Laboratory, Laurel, MD 20723

Thomas J. Horvath[6]
NASA Langley Research Center, Hampton VA 23681

Richard J. Schwartz[7]
Analytical Mechanics Associates, Hampton, VA 23681

Steven Tack[8]
Naval Air Warfare Center - Weapons Division, Pt. Mugu, CA 93042

Brett C. Bush[9]
Raytheon/Photon Research Associates, San Diego, CA 92121

A. Brandon Oliver[10]
NASA Johnson Space Center, Houston, TX

The Scientifically Calibrated In-Flight Imagery (SCIFLI) team captured high-resolution, calibrated, near-infrared imagery of the Orion capsule during atmospheric reentry of the EFT-1 mission. A US Navy NP-3D aircraft equipped with a multi-band optical sensor package, referred to as Cast Glance, acquired imagery of the Orion capsule's heatshield during a period when Orion was slowing from approximately Mach 10 to Mach 7. The line-of-sight distance ranged from approximately 65 to 40 nmi. Global surface temperatures of the capsule's thermal heatshield derived from the near-infrared intensity measurements complemented the in-depth (embedded) thermocouple measurements. Moreover, these derived surface temperatures are essential to the assessment of the thermocouples' reliance on inverse heat transfer methods and material response codes to infer the surface temperature from the in-depth measurements. The paper describes the image processing challenges associated with a manually-tracked, high-angular rate air-to-air observation. Issues included management of significant frame-to-frame motions due to both tracking jerk and jitter as well as distortions due to atmospheric effects. Corrections for changing sky backgrounds (including some cirrus clouds), atmospheric attenuation, and target orientations and ranges also had to be made. The image processing goal is to reduce the detrimental effects due to motion (both sensor and capsule), vibration (jitter), and atmospherics for image quality improvement, without compromising the quantitative integrity of the data, especially local intensity (temperature) variations. The paper will detail the approach of selecting and utilizing only the highest quality images, registering several co-temporal image frames to a single image frame to the extent frame-to-frame distortions would allow, and then co-adding the registered frames to improve image quality and reduce noise. Using preflight calibration data, the registered and averaged infrared intensity images were converted to surface temperatures on the Orion capsule's heatshield. Temperature uncertainties will be discussed relative to uncertainties of surface emissivity and atmospheric transmission loss. Comparison of limited onboard surface thermocouple data to the image derived surface temperature will be presented. This project was sponsored by the NASA Engineering Safety Center (NESC).

[1] Senior Professional Staff, Johns Hopkins University Applied Physics Laboratory.
[2] Principal Professional Staff, Johns Hopkins University Applied Physics Laboratory.
[3] Principal Professional Staff, Johns Hopkins University Applied Physics Laboratory.
[4] Senior Professional Staff, Johns Hopkins University Applied Physics Laboratory.
[5] Senior Professional Staff, Johns Hopkins University Applied Physics Laboratory.
[6] Aerospace Engineer, LaRC Aerothermodynamics Branch, AIAA Associate Fellow.
[7] Aerospace Engineer, LaRC Advanced Sensing and Optical Measurement Branch.
[8] Lead, Cast Glance Electro-Optical Systems and Flight Operations.
[9] Senior Professional Staff, Raytheon/Photon Research Associates.
[10] Aerospace Engineer, NASA Johnson Space Center.

I. Introduction

The Exploration Flight Test 1 (EFT-1) of the Orion Multi-Purpose Crew Vehicle occurred on December 5, 2014. The mission was a four hour, two orbit test of the Orion capsule, concluding with a high energy reentry at ~20,000 miles per hour during early daylight conditions. The flight test was intended to test various Orion systems, including the heatshield. The Orion heatshield was predominantly made of monolithic Avcoat, with the afterbody covered with Reaction Cured Glass (RCG) tiles. Avcoat is an ablative material also used on the Apollo capsules. The Orion heatshield was the largest of its kind ever built with a diameter of 198 inches and a thickness of about 1.6 inches. During EFT-1 reentry the heatshield surface temperature was expected to peak at approximately 4000 °F.

To evaluate the heating (and cooling) of the Orion heatshield, the SCIFLI (Scientifically Calibrated In-FLight Imagery) team prepared an ambitious plan to acquire imagery of the Orion capsule during its expected peak heating[1]. The SCIFLI team has multiple members from NASA and affiliated contractors, the Navy, and the Johns Hopkins University Applied Physics Laboratory (JHUAPL) to meet this challenge. The team had previously performed other reentry observation campaigns. These included seven Space Shuttle missions, a SpaceX Falcon stage one reentry, and a SpaceX Dragon capsule reentry. The prior shuttle observations resulted in many high spatial resolution temperature estimates of the shuttle windward surface at various times during its hypersonic reentry. These results were utilized to show full-scale surface temperatures as well as small-scale "speed bump" effects, to compare with on-board thermocouple data, to understand boundary layer transitions, and to help validate CFD simulations of hypersonic reentries [2-11]. However, the Orion capsule is much smaller in size than the space shuttle, making it more difficult to obtain sufficient resolution across the capsule to show spatial variations. In addition, the temperatures expected on the Orion heatshield were significantly higher than the highest observed on the space shuttle, which were approximately 2000 °F.

The Orion capsule was instrumented with thermocouples that were embedded into plugs at various depths in the 1.6 inch thick heatshield. Therefore, the thermocouples did not measure *surface* temperature, rather temperature at their embedded location. However, the surface temperature can be inferred from each thermocouple via inverse methods using material response code to account for ablation and surface recession. Surface temperature is a big factor in the amount of recession the heat shield experiences due to ablation. Although the image derived temperatures are intended to complement the subsurface thermocouples, a brief comparison of surface temperatures derived from selected "best" thermocouples will be made with the corresponding locations in the image derived temperatures.

The primary purpose of this paper is to highlight the aspects of processing the imagery acquired on the hypersonic portion of the Orion reentry for EFT-1 and show the results of the temperature estimates of the heatshield. This will include descriptions of data acquisition, data quality, data calibration, atmospheric compensation, estimates of Orion optical surface properties, as well as estimates of uncertainties for the image-derived temperature estimates. These results provide a better understanding of the Orion heatshield for future flights, especially EM-1 (Exploration Mission 1).

II. Data Acquisition Plan

Two Cast Glance aircraft, known by their call signs as Bloodhound 300 (BH-300) and Bloodhound 340 (BH-340), were flown to gather optical data on the Orion capsule for EFT-1. The optical data included wavelengths from visible through long-wave infrared during reentry interface, parachute descent, recovery, and splashdown. The primary data for this analysis was acquired by BH-300 during Orion reentry to estimate the heatshield temperature using the near-infrared (NIR) sensor, which is also the highest resolution sensor on Cast Glance. A description of the Cast Glance long-range optical sensor package is detailed in other references by Tack[4] and Zalameda[6]. Briefly, the primary sensor used for this analysis was a Prosilica GC1380 CCD camera (1360 x 1024 pixels, 12 bit pixel depth) with an 850nm long-pass cut-on filter used to collect imagery in the near-infrared wavelength region. The Cast Glance uses a gimbaled mirror for pointing and provides a field-of-view of approximately 0.285° x 0.215° in x and y dimensions, respectively. The pixel instantaneous field-of-view (IFOV) is approximately 3.6 microradians.

The mission plan was to obtain resolved imagery with the NIR sensor at the time when the Orion capsule heatshield was at its maximum temperature. Based on mission planning, this would occur when the capsule velocity is

approximately Mach 20.8 and the capsule altitude is approximately 159,000 feet (48.4 km). The Cast Glance would be positioned to acquire the capsule prior to this time as it comes above the viewing horizon. For long-range acquisition of the capsule, the short-wave infrared (SWIR) sensor would be utilized. Then the capsule would be tracked and observed as it flies toward and past the Cast Glance.

For the initial acquisition, the pre-mission radiance modeling indicated that acquiring the capsule might be challenging using the mid-wave infrared (MWIR) long range tracking system, which would typically be used. The capsule would be at exoatmospheric ambient temperature as it came over the horizon into view of the Cast Glance aircraft, which is not hot enough to provide a high signal-to-noise ratio (SNR) in the image. At that point, the aluminized Kapton tape on the heatshield would still be intact and highly reflective, so the radiance is dominated by solar reflection. This situation pointed towards the use of the SWIR system for initial acquisition and long range tracking. During the period of maximum heating, the NIR system would have no shortage of photons available, and either the use of a neutral density filter or reduced camera integration times (around 20 μsec) would be required. The analysis also clearly showed that the backshell would not generate enough photons for the NIR system to obtain a high enough signal at these integration times. So, if backshell temperature measurements were desired they would have to be made with the MWIR system, which has lower spatial resolution. The backshell temperature estimates were not a primary objective for this observation, and were not attempted for this analysis.

Another pre-mission analysis involved assessing the effect of ablation and shock layer radiation on the processed temperature estimates. The final outcome of the ablation study determined that while the shock layer radiation needed to be accounted for during the period of peak heating, the correction would be only on the order of three percent. This would be accounted for in the post-flight data processing, and would not alter the method of data acquisition. Ultimately, the Cast Glance aircraft had to position itself far down the trajectory from the peak heating location due to weather constraints at the originally planned Test Support Position. The imagery was acquired when the Orion capsule was at approximately Mach 10 instead of the planned Mach 21. Under these conditions the shock layer radiation and ablation of the heat shield were minimal, and these corrective factors were not required for the final data processing.

III. Summary of Data Collection and Initial Selections for Analysis

Imagery was collected for the EFT-1 mission, but not during peak heating as planned. During the time of reentry, there were high altitude clouds that prevented the Cast Glance from having a clear line-of-sight observation for the peak heating location. The SCIFLI team had contingency plans to reposition the Cast Glance aircraft, if possible, to a more favorable line-of-sight. For this case, the Cast Glance aircraft (BH-300) was repositioned downrange about 180 nmi to a later part of the reentry path, and the aircraft altitude was increased from the nominal 28,000 feet to approximately 33,000 feet.

Despite still having "broken" clouds in the repositioned area, the skilled and experienced Cast Glance team successfully acquired the Orion capsule and observed it for over 60 seconds during reentry. For the heatshield temperature analysis presented in this paper, there were approximately 900 unsaturated NIR images to evaluate covering the Orion capsule altitudes of 43 km to 41 km and Mach numbers of 9.9 to 7.6.

After the Orion capsule was acquired in the field of view of the NIR sensor, the integration time was quickly reduced by Cast Glance operators to avoid saturation of pixels. Collecting imagery at 30 Hz frame rate showed significant atmospheric effects due to air turbulence and thin clouds. There are also the unavoidable effects due to motion and vibration of the aircraft. Therefore, the image-to-image variations were even more evident than prior observations by Cast Glance, and it also resulted in fewer "lucky imaging" frames. Image-to-image variations frequently resulted in large (>1 pixel) apparent relative motions of the unresolved bright compression pads, and will be discussed in section IV. Prior discussions of image quality and selecting "lucky frames" are given for the previous space shuttle reentry observations[8,12].

To begin initial selections of imagery time segments, Figure 1 shows a plot of the overall trend during the observation for several image-derived parameters. The integrated capsule intensity, in raw sensor counts (left y-axis), is shown with a black line, and the sensor integration time, in milliseconds (right y-axis), is shown with a red line. The integration time was changed several times by the Cast Glance operators to accommodate the heatshield's

decreasing temperature during this part of the reentry. In the lower portion of the plot, the blue and light green lines show the average image intensity near the capsule that was used for background removal of intensity counts.

To select (or eliminate) time segments available for further radiometric analysis, several criteria were used. First, there must be no saturated pixels. Saturation only occurred during initial acquisition (prior to frame 7816). Second, there must be no indications of clouds in the line-of-sight. Near frame 8200 there was a large enough change in intensity to investigate if there were changes along the line-of-sight. The corresponding imagery from the mid-wave infrared (MWIR) sensor on Cast Glance, which has a wider FOV, confirmed an abrupt change in both the signal and foreground intensity corresponding to a thin cloud. Third, the imagery must be free from tracking motions, such as what occurs when the capsule is repositioned in the field-of-view, or is moving off the field-of-view such as frames ~8300-8430. Lastly, in the later frames past ~8700, the viewing geometry became too side-on to present good spatial coverage of the entire heatshield; therefore, this time range was also not selected.

Referring again to Figure 1, the dark green vertical lines in the plot represent the five selected time segments for further processing and analysis to estimate temperatures of the heat shield. The table on the right of the plot lists the frame numbers and GMT time stamps of the selected image frames. Several frames immediately before and after these five selected times were then chosen to enhance imagery as discussed in section IV.

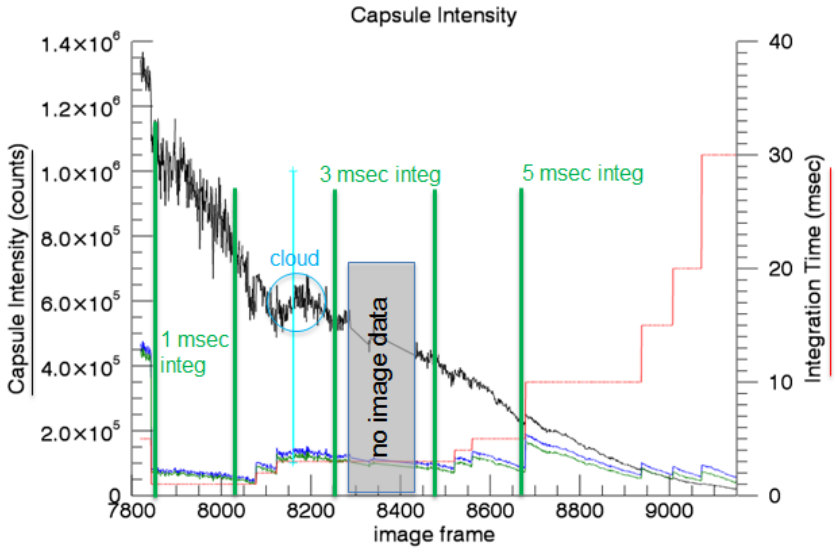

Selected Time Segments

NIR image frame number	GMT time stamp
7848	16:21:29.9917
8028	16:21:35.9798
8251	16:21:43.3983
8474	16:21:50.8271
8632	16:21:56.0939

Figure 1. Plot of several image-derived parameters to highlight selection of imagery for detailed analysis. Black line shows total capsule intensity. The thicker green vertical lines show selected time segments. Table on right shows frame number and time reference for the five selected time segments.

IV. Discussion of Data Quality and Image Selection

The image sets within the time segments selected were then further culled to include only those images that were judged to be "not smeared" due to tracking jerk and jitter and also having minimal distortions from atmospheric turbulence. These best images, or "lucky" images, are more amenable to further processing. In prior observations of the space shuttle, as many as 25 frames could be selected and co-registered for enhancing the imagery [8,12]. However, because the Orion capsule was much smaller than the shuttle (thus fewer pixels across), and this EFT-1 data collected had more image-to-image distortions, only 5 frames are used for each time segment in the post processing. We attempted to identify the very best images in the data set, i.e., ones that appeared relatively undistorted, by evaluating the six highly distinct compression pads.

At this point, it would be helpful to describe the physical structure of the compression pads that cause higher heating than the rest of the heatshield. In the region of each compression pad there is thickening of the Avcoat around the entire pad creating a shallow ramp and cavity. The pad itself is circular (~9.5 inch diameter) and made from carbon phenolic with a stainless steel bolt and insert at the pad center. The metal bolt/insert is ~2.75 inches in diameter. The planform shape created by intersection of the ramps with the smooth outer mold line (OML) geometry are oblong on the as-flown geometry. The Avcoat on the acreage OML and ramps surrounding the pads is identical material but there is definitely a material and density difference between the surrounding Avcoat and carbon-phenolic/metal comprising the actual pads.

For image selection, the indicators of the least distorted images were the best "point-like" response from the compression pads, as well as using the relative distances between the compression pads. Only these so-called "lucky images" were processed to represent the spatial variations and the temporal evolution of temperatures. In addition, the Orion flight data was examined to avoid images that might be altered by the Reaction Control System (RCS) thruster firings from the capsule. Note that thruster firings were not easily apparent in the imagery, and the thruster locations on the backshell were also obscured from view by the heatshield while the capsule was primarily head-on. An example of the 5 frames selected for post processing of frame 8028 is shown in Figure 2. Note that each of these is a 32x32 pixel subimage of the full image of the NIR sensor centered on the capsule. The time progression is shown from right to left.

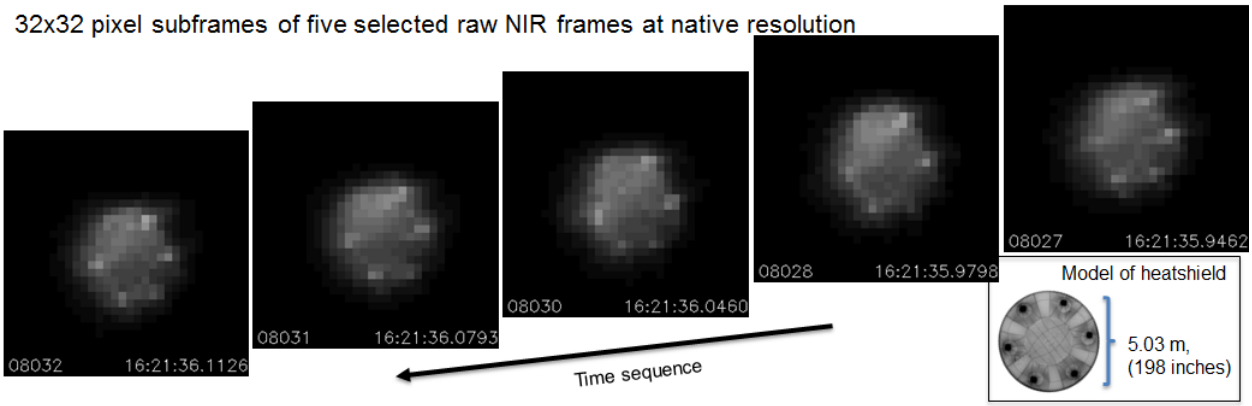

Figure 2. The selected 5 frames used to post-process imagery for frame 8028. The angle between the line-of-sight and heatshield normal of Orion capsule is approximately 33°.

Orion's apparent diameter of approximately 12 to 13 pixels during this selected time interval yielded a scale of ~15 inches/pixel, as expected for the line-of-sight range of 57 nautical miles (nmi). As mentioned earlier, the higher heating "points" at the locations of the compression pads and/or their center posts are very noticeable. These hotter features are unresolved, because they are smaller than the pixel footprint in these images. However, if it is actually the excess heat from the posts that we are observing, then the actual temperature differences between the posts and their immediate surroundings would be well in excess of the ~100 °F observed difference in the imagery. The pads/posts also can be used to infer the capsule's orientation, in particular the direction of its Z-axis ("capsule up") which we know to be parallel to two of the posts. Given the observing geometry in this example, then "up" should be close to the 11:30 o'clock position. However, we know that Orion was being "flown" in an energy-management turn to the right at this time of the reentry. The observation of the warmer region toward the upper left quadrant of the capsule (near 10:00-11:00 o'clock position) appears consistent with the reported bank angle of 22°.

V. Summary of Processing Steps

Figure 3 is a diagram summarizing the processing steps to derive 2D temperature images of heatshield surface. The goal is to produce the highest quality images with the lowest possible temperature uncertainties. The primary data sources (or "inputs") specific to the EFT-1 mission are shown as dashed rectangles with rounded edges, which are calibration data, mission data, weather model data, emissivity estimate, and best estimated trajectory. The four main areas of the processing are shown by the solid lined rectangular boxes. The topics described in this section are: A) improvement of image quality, B) radiometric calibration, C) atmospheric compensation, D) surface emissivity.

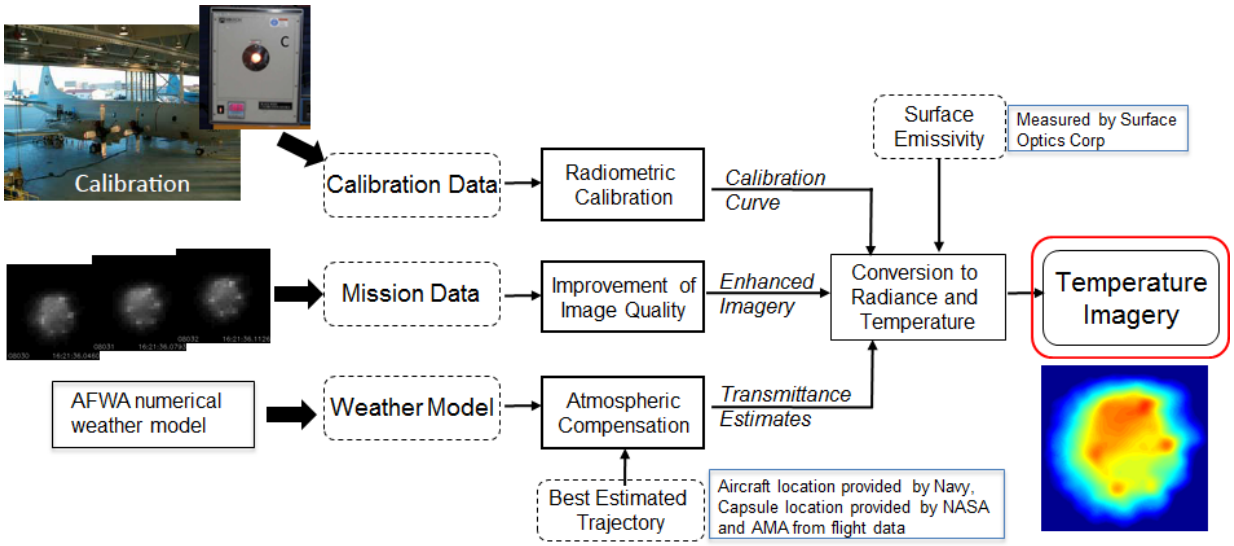

Figure 3. Summary of data sources and process for calculating temperature imagery.

A. Improvement of Image Quality

After the five best images for each time segment were selected as described in section IV, image quality was improved prior to converting the data to radiometric units (i.e., radiance). First, each image was "over-resolved" via interpolation by a factor of 8 to optimize further image processing. We then co-registered each of the five "interpolated" frames to a single frame using the algorithm developed by Periaswamy[13]. Finally, we averaged the five co-registered images expecting to achieve both a factor of two increase in signal-to-noise – and thus improved temperature accuracy – as well as an increase in resolution of spatial features.

Figure 4 shows the five "interpolated" frames and the single co-registered image at the bottom. In the interpolated images, the image-to-image variations are even more apparent with more spatial detail than the raw images of Figure 2. The resulting co-registered image is a well enhanced image while maintaining the radiometric integrity of the data. A more detailed discussion on this processing has been described in prior publications[8,12].

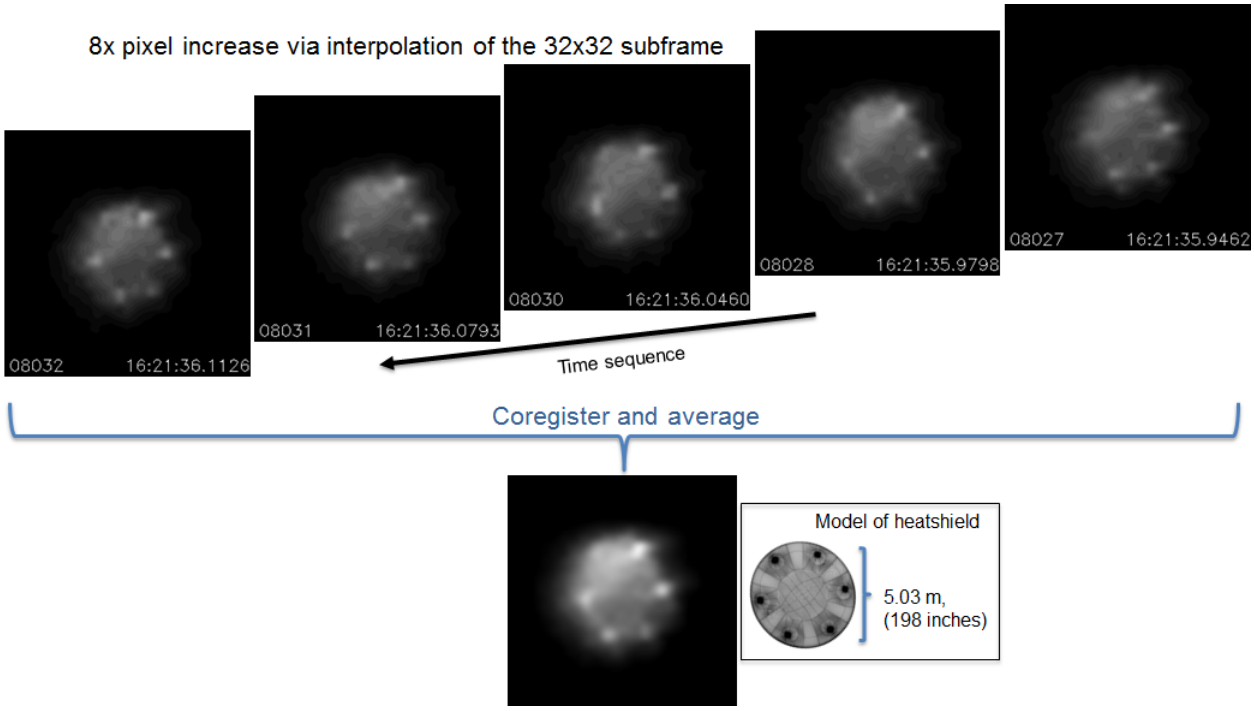

Figure 4. The selected 5 frames used to post-process imagery for frame 8028, after the 8x interpolation, showing more defined compression pads/posts. The bottom image shows the result after co-registration and averaging of the 5 frames.

B. Radiometric Calibration

The sensor calibrations took place at Point Mugu Naval Air Station in Ventura County, CA two days prior to the EFT-1 mission. Image data were captured of calibrated blackbody sources by the Cast Glance sensor operators for several different integration times. Then the data was analyzed to determine the counts, or digital numbers (DNs), for each integration time. The result of the calibration analysis is a coefficient relating the sensor counts (DNs) to the in-band radiance (in W/cm²/sr) at the sensor's aperture for a particular integration time.

The calibration analysis first requires extracting the pixel values in digital numbers generated by the source radiance(s) within the image. In this instance, the calibration sources are blackbodies whose radiances are controlled by their temperatures and emissivities. Multiple frames at each integration time are recorded and then averaged to reduce the errors caused by sensor noise. Sensor background values are also calculated and subtracted from the pixel values generated by the source radiance. Also, the line-of-sight distance of about 450 feet and the atmospheric conditions at the time of calibration were recorded and used as inputs for a MODTRAN calculated atmospheric transmittance for our calibration measurement configuration. This is necessary to compensate for atmospheric transmission loss along the line-of-sight for the calibration result.

Then the sensor's background subtracted count rate is computed for all integration times at each blackbody setting. A visual check is performed to assure that the sensor's response (count rate in DN/sec) is actually linear with in-band radiance. After verifying linearity, a linear least squares fit is performed between the background subtracted count rate and the in-band radiance. For the NIR sensor, the slope (force zero intercept) is 4.957×10^{7} making the calibration coefficient (the reciprocal of the slope) 2.017×10^{-8}. The appropriate units for the calibration coefficient are: (W/cm²/sr) / (DN/sec). The calibration coefficient when converting directly from count rate into in-band radiance is:

$$Inband\ Radiance\ \left(\frac{Watts}{cm^2 \cdot sr}\right) = 2.017 \times 10^{-8} * Count\ Rate\left(\frac{DN}{sec}\right)$$

As mentioned earlier, the Cast Glance sensor operators adjust the NIR sensor's integration time during the mission, attempting to optimize the target DNs for signal-to-noise ratio and also to prevent saturation. Accordingly, given the

sensor's finite dynamic range imposed by the 12-bit analog to digital convertor, each integration time enables calibrated data on the target of interest to be captured over a limited range of surface temperatures. The blackbody temperature for the entire 12-bit range of ADC counts for three representative integration times is given below in Figure 5. This figure represents the range of integration times used during the collection of the NIR imagery. This emphasizes the need for changing integration times to yield enough signal counts as the temperature of the capsule dropped a few hundred degrees Fahrenheit during the observation of slightly more than 60 seconds.

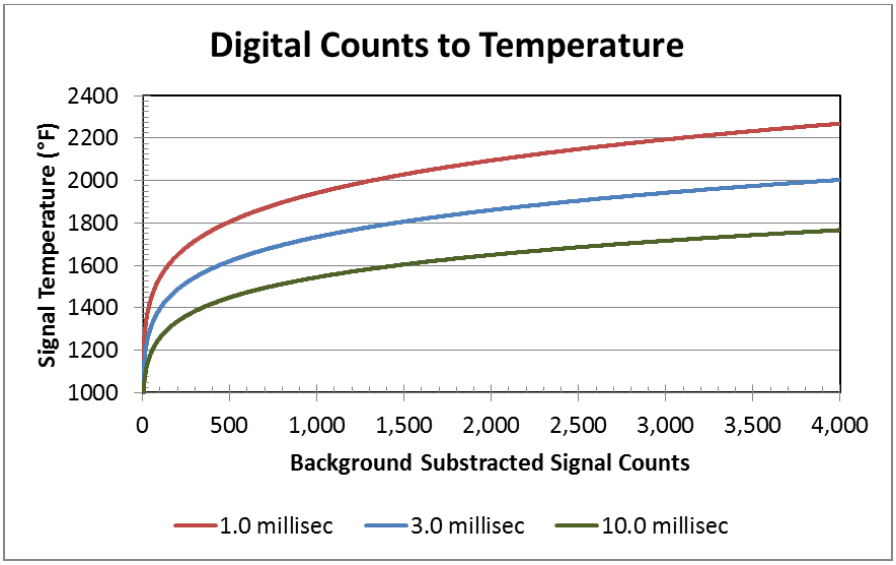

Figure 5: Based on calibration analysis, this plot shows the temperature given the 12-bit ADC value (0-4095 counts) at three integration times for the NIR sensor used in the mission data collection.

C. Atmospheric Compensation

Along the line-of-sight path from the capsule to the sensor, the received light incurs a small transmission loss in the atmosphere due to the scattering and absorption. A tool was developed at JHUAPL called ACS (Atmospheric Compensation System) to perform these calculations[14]. The atmospheric data were taken from the Air Force Weather Agency's (AFWA) 3D numerical weather model and were obtained within the nearest hour of the data collection. The spectral band of the CCD sensor with 850 nm cut-on filter was approximated as a top-hat (flat) response from 0.843 to 1.1 microns, which is adequate for the transmittance calculations.

The average in-band transmittance is computed for each image frame time using MODTRAN with the observing geometry (capsule and aircraft locations) and the atmospheric data available. The data contained in the 3D meteorological data cube are traversed along the line-of-sight to determine the respective atmospheric transmittance. For typical conditions above 33,000 feet altitude and a nominal 57 nmi range at 17° elevation angle, the transmittance is usually around 0.96. This 4% transmission loss is relatively small, but it must still be included to accurately estimate radiance from the capsule and then the surface temperatures. The effect of the transmission loss uncertainty on the temperature estimates is discussed in section VIII.

D. Surface Emissivity

Prior to the mission, Surface Optics Corporation performed several measurements to determine emissivity ε of the heatshield. As mentioned in Section I, the heatshield surface is Avcoat, which can become charred and can also ablate during the mission. Therefore, the emissivity measurements were made for both a virgin Avcoat sample and a charred Avcoat sample. For the imagery data processed, the reentry was past peak heating and cooling, therefore, the heatshield surface was certainly charred at this time during the reentry. Figure 6 shows a plot of the estimated emissivity of the charred Avcoat sample in the waveband regions for three Cast Glance infrared sensors. The blue line shows the result for the NIR sensor from which the surface temperatures are determined. The emissivity only changes slightly as the angle increases, which allows us to assume a constant emissivity over the entire heatshield

even though it is a curved surface. However, as the line-of-sight angle to the heatshield normal changes during the observation (from ~11-53°), we adjust the emissivity value slightly to calculate the surface temperatures.

Other laboratory measurements were conducted to determine the emissivity of charred Avcoat while at a representative reentry temperature. These emissivity estimates indicated a value between 0.8 and 0.82. The impact of this uncertainty in the emissivity is discussed in section VIII.

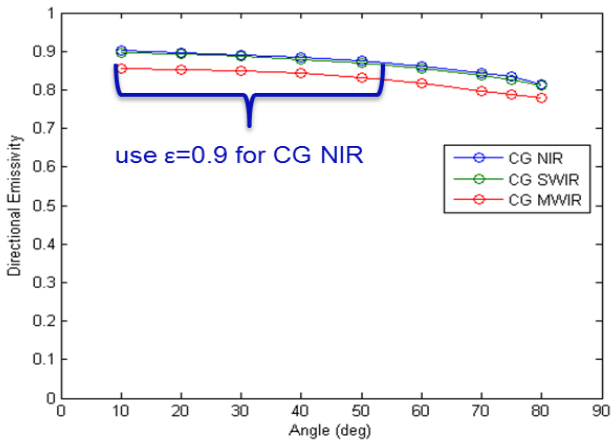

Figure 6. Emissivity ε estimated within the Cast Glance sensor wavebands of a charred Avcoat sample based on laboratory measurements.

VI. Images of Estimated Temperatures

Table 1 shows the resulting temperature image estimates for the five selected time segments along with some parameters of interest. The imagery is shown on the same temperature scale (lower left of Table 1), clearly indicating the rapid cooling (~300° F in 36 seconds) of the heatshield during the observation. The capsule changed orientation slightly as observed by locations of the compression pads as well as from the flight parameters. The primary flight dynamic during the observation, for the most part, was that the capsule was slowing rapidly. The viewing geometry was nearly head-on for the first image shown (frame 7848) and gradually became more side-on.

Table 1. Final temperature image results for five selected times along with some relevant parameters for each frame time.

Image Frame Number:	7848	8028	8251	8474	8632
Image Frame Time Reference (GMT):	16:21:29.9917	16:21:35.9798	16:21:43.3983	16:21:50.8271	16:21:56.0939
Mach number:	9.91	9.33	8.66	8.04	7.63
Target Range (nmi):	65.1	57.2	49.2	43.3	40.6
Target elevation (deg):	15.4	17.4	20.2	22.7	24.1
Raw Image Pixel Footprint (inches):	17.1	15.0	12.9	11.4	10.7
Capsule apparent pitch (angle of attack;deg):	-19.1	-19.1	-19.2	-19.4	-19.4
Capsule "up" (reference to z-axis; deg):	18	18	18	-7	-9
Capsule bank angle (deg):	30.39	22.21	27.85	38.48	46.46
Angle of l.o.s. to heatshield normal(deg):	11.5	33.5	36.0	44.0	53.0
Peak temperature (deg F):	1940	1843	1760	1718	1643
Minimum temperature (deg F):	~1720	~1630	~1520	~1480	~1400
Temperature (deg F): 1400 1500 1600 1700 1800 1900	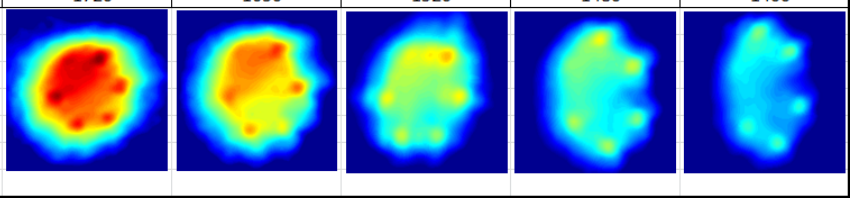				

VII. Comparison of Image Derived Temperatures to Surface Temperatures Reconstructed from Thermocouples

Instrumented plugs were installed at multiple points on the Avcoat heatshield to measure the in-depth temperatures during the EFT-1 entry. The plugs considered in the present work consisted of two Type-S thermocouples, two Type-K thermocouples, and a HEAT recession sensor [15]. The Type-S thermocouple (TC) nearest the surface was installed nominally 0.1 in below the Avcoat surface with the remaining TCs installed at progressively deeper locations. Junction location and TC depths were verified by X-ray prior to installation in the heatshield. Reconstruction of Avcoat surface temperatures using the near-surface TC measurements was performed using the inverse heat transfer capabilities of the CHAR code and the design Avcoat response model [16,17].

Figure 7 shows the thermocouple locations and an example of temperatures extracted for frame 7848. Based on the known locations of the thermocouples, the corresponding locations in the imagery are estimated by using the image pixel size references. The raw imagery for this example had a resolution of ~15 inches/pixel, while the final imagery shown in the lower left is "interpolated" by a factor of 8, resulting in slightly less than 2 inches/pixel. The two thermocouple locations (plug06 and plug08) were selected based on having the highest quality thermocouple data and also away from an edge of the heatshield surface. The line profile across the 2D temperature image in the lower plots is a pixel-by-pixel plot across the image rotated to correspond to the upper left diagram.

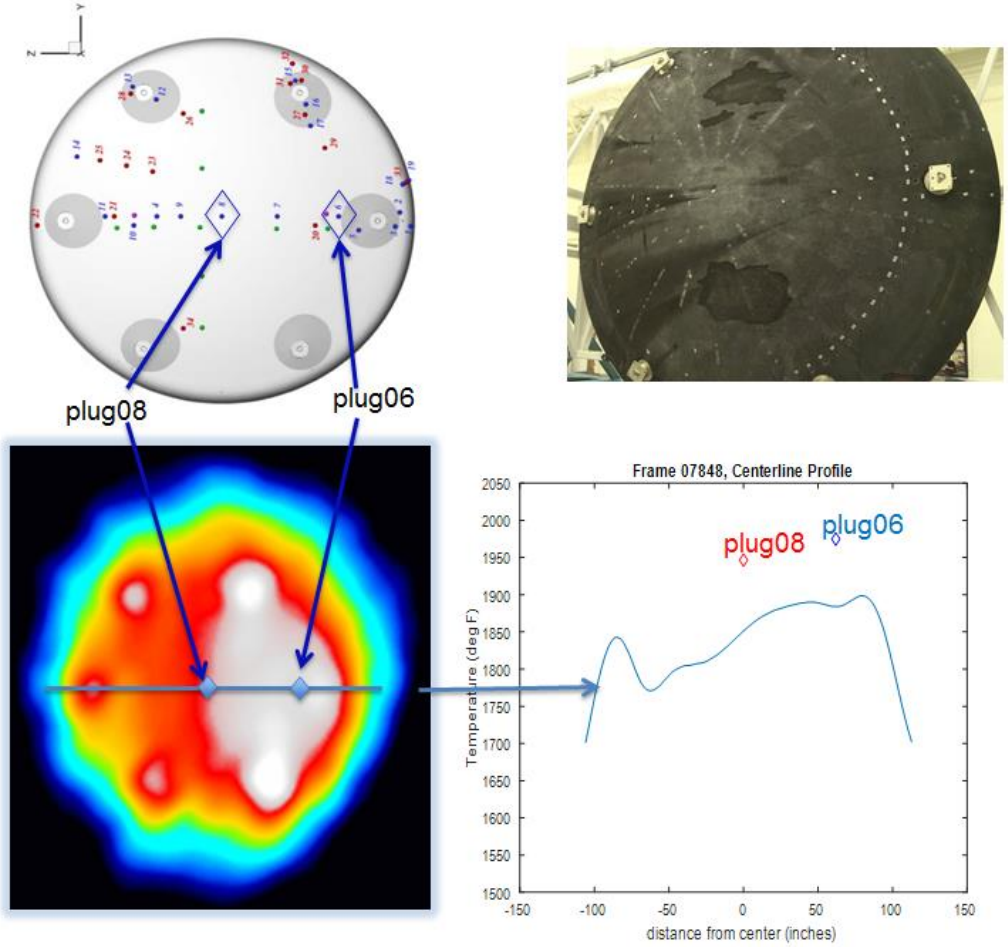

Figure 7. Summary of the thermocouple locations used and the corresponding image locations in frame 7848 for a comparison of estimated temperatures. Upper left shows diagram of all instrumentation locations, with blue diamond shapes over the two selected thermocouple locations. Upper right shows photograph of heatshield post mission only as a visual reference. Lower left shows the temperature image for frame 7848 (note different color scale) that has been rotated to correspond to the instrumentation diagram of upper left. Lower right is a profile plot across the temperature image with a diamond shape overlay of temperatures derived from plug06 and plug08 thermocouples.

Table 2 shows the temperature estimates of the two thermocouple locations for the five selected image times. The last two rows of text show the differences. The imagery estimates were consistently lower than the temperatures derived from the thermocouples. Most of the differences were in the range of 100 °F. Some further discussion is given in the next section when describing the uncertainties.

Table 2. Comparison of temperatures for plug06 and plug08 locations for the five selected time segments.

Image Frame Number	7848	8028	8251	8474	8632
Image Frame Time Reference (GMT)	16:21:29.9917	16:21:35.9798	16:21:43.3983	16:21:50.8271	16:21:56.0939
Mach number	9.91	9.33	8.66	8.04	7.63
Orion Time Reference (GMT)	16:21:29.846	16:21:35.846	16:21:43.271	16:21:50.696	16:21:55.946
Thermocouple Time (MET_wrt_CMSep)	3173.526	3179.526	3186.951	3194.376	3199.626
TC Derived Temperature for Plug06 TC (°F)	1975	1891	1797	1712	1659
TC Derived Temperature for Plug08 TC (°F)	1947	1860	1755	1672	1619
Image Derived Temperature for Plug06 (°F)	1886	1798	1702	1655	1596
Image Derived Temperature for Plug08 (°F)	1846	1738	1640	1580	1530
Δ between Plug06 Image and TC estimates (°F)	-89	-93	-95	-57	-63
Δ between Plug08 Image and TC estimates (°F)	-101	-122	-115	-92	-89
Temperature (deg F): 1400 1500 1600 1700 1800 1900	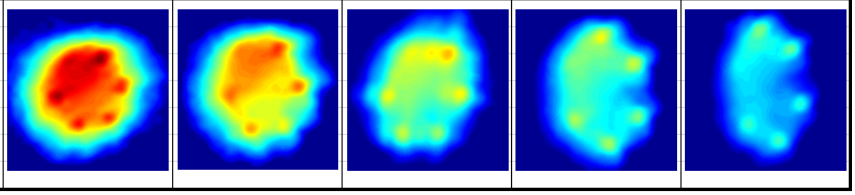				

Even though there was a bias between the two different temperature estimates, there was relative consistency across the five time segments because both show a rapidly decreasing temperature trend. To further evaluate how the imagery captured the "trend" of the temperature, we evaluated a single location, plug08, during all time periods with good imagery data. The selection of time segments for this analysis was similar to selecting best image time segments described in section III. We skipped times when there was excessive blur or no image data, interference from clouds, and large integration time changes. Figure 8 shows the same plot as shown earlier in Figure 1 and overlays in light blue-gray boxes the time segments when a good "single point" temperature can be calculated at the location of plug08, which is the center of the heatshield. For each frame in these time segments, the raw imagery was processed "as is" (no imagery enhancement), and the temperature of the center pixel of the heat shield was computed. The changing transmittance along the line-of-sight path was also accounted for even though there were only minor changes.

The imagery estimates of temperature for plug08 location were compared to the reconstructed temperature estimates for plug08 from the thermocouple data. Figure 9 shows a plot of these calculations, with the red line showing temperatures derived from thermocouple data (note that some artifacts and spikes were smoothed out) and the blue dots show the temperature estimates for each frame. The slope for each estimate was fitted to a line for the two time segments, although during the full observation the temperature did not decrease linearly. The cyan colored line is the linear fit of the image derived temperatures, and the bold red line is the linear fit of the thermocouple derived temperature. The resulting linear slopes for each time segment correlate reasonably well, indicating that the change in temperature, or cooling rate, was well represented by both methods.

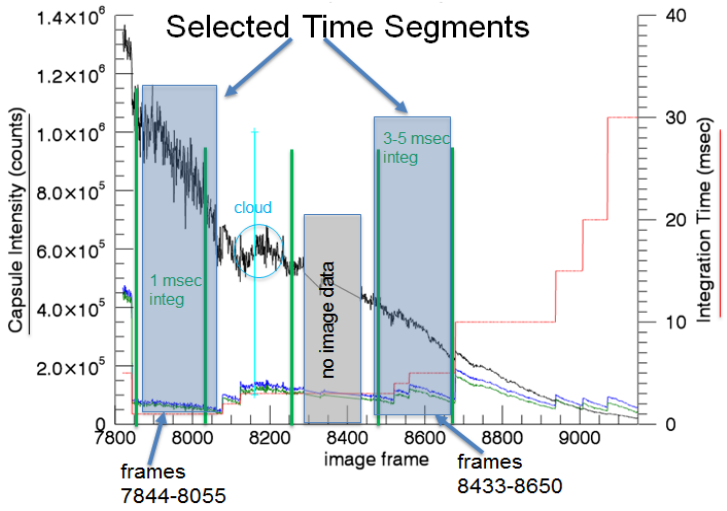

Figure 8. Plot (from Figure 1) showing selection of two time segments shaded in blue for comparison of cooling rates.

Because the image derived temperature estimates shown by blue dots were not smoothed, this gives a representation of the "noise" in the imagery estimates. The first time segment had larger variations than the second time segment for two reasons. One reason was that there was a larger intensity gradient (larger temperature change) across the center of the capsule during the earlier time segment, so the discretization of pixels along that large gradient causes variations. The second reason is that the integration time was larger for the second time segment, which tends to reduce or smooth the frame-to-frame "noise", similar to co-adding frames.

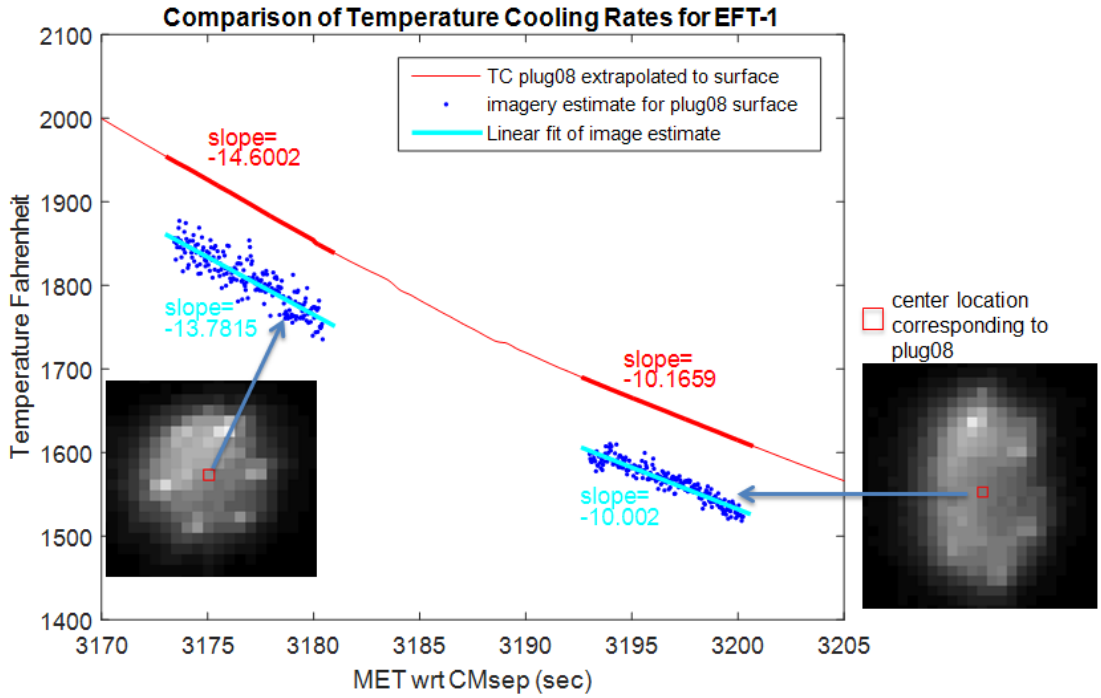

Figure 9. Comparison of temperature cooling rates during selected intervals of reentry when best imagery was acquired. Red line shows the surface temperature estimate derived from the thermocouple at the center of the heatshield (plug08). Blue dots show temperature estimates derived from imagery, along with two sample images and the center pixel highlighted in red. Note that the slopes of linear fits in the two segments correlate.

VIII. Uncertainty of Temperature Estimates

The final temperature image is a result of the series of calculations summarized earlier, and most of calculations have corresponding uncertainties. There are four sources of the uncertainties: sensor noise (measurement noise), radiometric calibration, emissivity, and atmospheric transmittance. To assess a total uncertainty, we assumed a realistic "worst case" for each of these within the configuration used for the EFT-1 mission, and then combined them in quadrature. The total uncertainty for these temperatures is estimated to be +/-15 °F. This is consistent with prior uncertainty estimates for airborne data collections described in earlier work[6,8].

The measurement noise (after co-adding 5 frames) can contribute up to approximately 6 °F, based estimates from prior work [8,12]. The radiometric calibration uncertainty is quite good, and it has been estimated to contribute ~2 °F. The uncertainty of the emissivity estimate is somewhat difficult to quantify because of the unknowns regarding the condition of the Avcoat. Lab measurements on different samples resulted in values from 0.8-0.9. Individual test materials did show a relatively consistent emissivity value across the infrared wavebands and for different viewing angles, therefore, we assumed the uncertainty in the emissivity should be within 5%. This 5% error would account for an error of approximately 10 °F. Even a 10% error on the emissivity value would only increase the error to ~20 °F. Lastly, the uncertainty of the atmospheric transmittance is also somewhat difficult to know, because the exact line-of-sight conditions during the observation are not well known. However, at the altitudes of the aircraft and capsule, the transmittance is fairly consistent at approximately 0.96, and typically does not change more than a few percent. As a worst case, we assume a larger transmittance uncertainty of 5%, which then causes an uncertainty of ~10 °F.

The total uncertainty of +/-15 °F is significantly smaller than the ~100 °F difference in the temperatures derived from the imagery and the thermocouples. Even a straight addition of the various contributors to uncertainties in the imagery estimates would only approach a 30 °F uncertainty. The surface temperatures derived from the in-depth thermocouples do have several uncertainties as well, both due to sensors as well as the inverse methods utilized to calculate the temperatures. These derivations were completed by engineers at the NASA Johnson Space Center [15,16]. It is beyond the scope of this paper to thoroughly consider all of the reasons for an ~100 °F bias between the two temperature estimates.

IX. Concluding Remarks

The process of generating 2-D thermography of the Orion heatshield during hypersonic reentry has been presented. The Cast Glance sensor system acquired NIR images from Mach 10 to Mach 7 at spatial resolutions of around 10 to 17 inches per pixel. By selecting the best images, enhancing them while maintaining quantitative integrity, applying radiometric calibration conversion, and adjusting for the atmospheric transmittance along the line-of-sight and the optical surface properties, relatively accurate temperature estimates were made of the heatshield surface.

The resulting surface temperature images should be a good resource for evaluating the heatshield and also for comparing with flight data and embedded thermocouple measurements. The direct comparison with surface temperatures derived from inverse methods using material response code to account for ablation and surface recession yielded a bias of about 100 °F. The temperature trend during the observation was very similar between the image-based estimates and the thermocouple derived estimates.

Acknowledgements

The JHUAPL authors would like to gratefully acknowledge NASA for financial support of this work through contract NNN06AA01C. Thanks to several NASA members: Stan Bouslog for providing surface material samples in order to make emissivity measurements of Avcoat, C. David Mercer for data management and handling, and to Karen Bibb for providing Orion EFT-1 flight data. The SCIFLI project involved numerous other members not mentioned as co-authors, and their contributions are greatly appreciated. The team is a top-notch crew and justifiably has been given a NASA Engineering and Safety Center Group Achievement Award.

X. References

[1] Horvath, T. J., Rufer, S. J., Schuster, D. M., Mendeck, G. F., Oliver, A. B., Schwartz, R. J., Verstynen, H. A., Mercer, C. D., Tack, S., Ingram, B., Spisz, T. S., Taylor, J. C., Kennerly, S.W., Kwame, O. W., "Infrared Observations of the Orion Capsule During EFT-1 Hypersonic Reentry", 46th AIAA Thermophysics Conference; 13-16 Jun. 2016; Washington, DC.

[2] Horvath, T. J., Tomek, D. M., Berger, K. T., Zalameda, J. N., Splinter, S. C., Krasa, P. W., Schwartz, R. j., Gibson, D. M., Tietjen, A. B., Tack, S., "The HYTHIRM Project: Flight Thermography of the Space Shuttle During Hypersonic Re-entry," AIAA-2010-241, January 2010.

[3] Anderson, B., Campbell, C., Kinder, J., Saucedo, L., "Boundary Layer Transition Flight Experiment Overview and In-Situ Measurements," AIAA-2010-240, January 2010.

[4] Tack, S., Tomek, D. M, Horvath, T. J., Verstynen, H. A., Shea, E. J., "Cast Glance Near Infrared Imaging Observations of the Space Shuttle During Hypersonic Re-entry," AIAA-2010-243, January 2010.

[5] Gibson, D. M., Spisz, T. S., Taylor, J. C., Zalameda, J. N., Horvath, T. J., Tomek, D. M., Tietjen, A. B., Tack and Bush, B. C., S.,"HYTHIRM Radiance Modeling and Image Analyses in Support of STS-119, STS-125 and STS-128 Space Shuttle Hypersonic Re-entries," AIAA-2010-244, January 2010.

[6] Zalameda, J. N., Horvath, T. J., Tomek, D. M., Tietjen, A. B., Gibson, D. M., Taylor, J. C., Tack, S., Bush, B. C., Mercer, C. D., and Shea, E. J., "Application of a Near Infrared Imaging System for Thermographic Imaging of the Space Shuttle During Hypersonic Re-Entry," AIAA-2010-245, January 2010.

[7] Wood, W. A., Kleb, W. L., Tang, C. Y., Palmer, G. E., Hyatt, A. J., Wise, A. J., McCloud, P. L., "Comparison of CFD Predictions with Shuttle Global Flight Thermal Imagery and Discrete Surface Measurements," AIAA-2010-454, January 2010.

[8] Spisz, T. S., Taylor, J. C., Gibson, D. M., Kwame, O. W., Horvath, T. J., Zalameda, J. N., Tomek, D. M., Berger, Tietjen, A. B., Tack, S., and Schwartz, R. J., "Processing near-infrared imagery of hypersonic space shuttle reentries," Thermosense XXXII Conference at 2010 SPIE Defense, Security, and Sensing Symposium, 5-9 April 2010, Orlando, FL, Paper 7661-17.

[9] Berger, K. T., Anderson, B. P., Campbell, C. H., Garske, M. T., Saucedo, L. A., Kinder, G. R., and Micklos, A. M., "Boundary Layer Transition Flight Experiment Overview," 42nd AIAA Thermophysics Conference, American Institute of Aeronautics and Astronautics, Reston, VA, June 2011.

[10] Schwartz, R. J., McCrea, A. C., Gruber, J. R., Hensley, D. W., Verstynen, H. A., Oram, T., Berger, K. T., Splinter, S., Horvath, T. J., and Kerns, R. V., "Remote Infrared Imaging of the Space Shuttle During Hypersonic Flight: HYTHIRM Mission Operations and Coordination," 42nd AIAA Thermophysics Conference, American Institute of Aeronautics and Astronautics, Reston, VA, June 2011.

[11] Horvath, T. J., Kerns, R. V., Jones, K. M., Grinstead, J. H., Schwartz, R. J., Gibson, D. M., Tack, S., Dantowitz, R. F., "A Vision of Quantitative Imaging Technology for Validation of Advanced Flight Technologies," 42nd AIAA Thermophysics Conference, American Institute of Aeronautics and Astronautics, Reston, VA, June 2011.

[12] Spisz, T. S., Taylor, J. C., Kennerly, S.W., Kwame, O. W., Gibson, D. M., Horvath, T. J., Zalameda, J. N., Kerns, R.V., Shea, E.J., Mercer, C.D., Schwartz, R. J., Dantowitz, R.F., Kozubal, M.J, "Processing ground-based near-infrared imagery of space shuttle reentries," Thermosense XXXIV Conference at 2012 SPIE Defense, Security, and Sensing Symposium, 23-27 April 2012, Baltimore, MD, Paper 8354-15.

[13] Periaswamy, S., Farid, H.. "Elastic registration in the presence of intensity variations", IEEE Transactions on Medical Imaging, vol.22 no.7, July 2003.

[14] Kelly, M.A., Osei-Wusu, K., Spisz, T.S., Strong, S., Setters, N., Gibson, D.M., "Assimilation of nontraditional datasets to improve atmospheric compensation," Atmospheric Propagation IX Conference at 2012 SPIE Defense, Security, and Sensing Symposium, 23-27 April 2012, Baltimore, MD, SPIE Vol 8380.

[15] Santos, J., Oishi, T., Martinez, E., "Isotherm Sensor Calibration Program for Mars Science Laboratory Heat Shield Flight Data Analysis", 42nd AIAA Thermophysics Conference, 27-30 June 2011, Honolulu, Hawaii, AIAA 2011-3955.

[16] Oliver, A. B., Amar, A. J., Droba, J., Lessard V., Mahzari, M. "EFT-1 Heatshield Aerothermal Environment Reconstruction", 46th AIAA Thermophysics Conference; 13-16 Jun. 2016; Washington, DC.

[17] Oliver, A. B., Amar, A. J., "Inverse Heat Conduction Methods in the CHAR Code for Aerothermal Flight Data Reconstruction", 46th AIAA Thermophysics Conference; 13-16 Jun. 2016; Washington, DC.